Advances in Experimental Medicine and Biology 1269

Edwin M. Nemoto · Eileen M. Harrison
Sally C. Pias · Denis E. Bragin
David K. Harrison · Joseph C. LaManna *Editors*

Oxygen Transport to Tissue XLII

Springer

Advances in Experimental Medicine and Biology

Volume 1269

Advances in Experimental Medicine and Biology provides a platform for scientific contributions in the main disciplines of the biomedicine and the life sciences. This series publishes thematic volumes on contemporary research in the areas of microbiology, immunology, neurosciences, biochemistry, biomedical engineering, genetics, physiology, and cancer research. Covering emerging topics and techniques in basic and clinical science, it brings together clinicians and researchers from various fields.

Advances in Experimental Medicine and Biology has been publishing exceptional works in the field for over 40 years, and is indexed in SCOPUS, Medline (PubMed), Journal Citation Reports/Science Edition, Science Citation Index Expanded (SciSearch, Web of Science), EMBASE, BIOSIS, Reaxys, EMBiology, the Chemical Abstracts Service (CAS), and Pathway Studio.

2019 Impact Factor: 2.450 5 Year Impact Factor: 2.324.

More information about this series at http://www.springer.com/series/5584

Edwin M. Nemoto • Eileen M. Harrison
Sally C. Pias • Denis E. Bragin
David K. Harrison • Joseph C. LaManna
Editors

Oxygen Transport to Tissue XLII

Springer

Editors
Edwin M. Nemoto
Department of Neurosurgery
University of New Mexico
Albuquerque, NM, USA

Sally C. Pias
Department of Chemistry
New Mexico Institute of Mining and Technology (New Mexico Tech)
Socorro, NM, USA

David K. Harrison
St. Lorenzen, Italy

Eileen M. Harrison
Bozen, Italy

Denis E. Bragin
Lovelace Biomedical Research Institute
Albuquerque, NM, USA

Joseph C. LaManna
Department of Physiology & Biophysics
Case Western Reserve University
School of Medicine
Cleveland, OH, USA

ISSN 0065-2598 ISSN 2214-8019 (electronic)
Advances in Experimental Medicine and Biology
ISBN 978-3-030-48236-7 ISBN 978-3-030-48238-1 (eBook)
https://doi.org/10.1007/978-3-030-48238-1

This Springer imprint is published by the registered company Springer Nature Switzerland AG
The registered company address is: Gewerbestrasse 11, 6330 Cham, Switzerland

Preface

Hypnos and the Flame
(original photograph courtesy of Dr. John W. Severinghaus)

In his foreword to John Nunn's book *Applied Respiratory Physiology*, John Severinghaus, an anesthesiologist and also my postdoctoral mentor as a Fellow at the Cardiovascular Research Institute at the University of California, San Francisco, wrote the following under the title "A Flame for Hypnos."

> The lighted candle respires and we call it flame. The body respires and we call it life. Neither flame nor life are substance, but process. The flame is as different from the wick and wax as life from the body, as gravitation from the falling apple or love from a hormone. Newton taught science to have faith in processes as well as substance-to compute, predict and depend upon an irrational attraction.

Such has been our study of oxygen, the substance in the whole of physiology and clinical medicine from the air we breathe to its consumption at the level of the mitochondrion for the past 47 years since 1973 when the International Society of Oxygen Transport to Tissue (ISOTT) was founded.

Although this 47th Annual meeting of our society began under the duress of a shortened time scale, we were able to host approximately 95 participants to enjoy the sunshine and American Indian Culture here in the Midwest,

where art is king. We enjoyed the company and presentations of all the attendees and hope that all had an excellent experience in New Mexico and Albuquerque.

Department of Neurosurgery
University of New Mexico,
Albuquerque, NM, USA

Edwin M. Nemoto

In Memoriam

Laraine Visser

"To my loved ones, I thought it might be nice if—later on—in your own time and in a place that you like, you might want to celebrate (my) life. You could do this alone, or with someone else that we shared good times with… with love as always. Laraine "Larry" Visser-Isles".

For well over 20 years Laraine Visser was present at every ISOTT meeting cheerfully sitting at the manuscript desk accepting submissions for the proceedings, offering advice and reminding authors about the other documents the publisher required to accompany their papers. She was also a very lively and popular participant in the meetings' social events. Fifteen years ago she managed to persuade me to volunteer to take on the scientific editing of the book in order to ensure the smooth flow of manuscripts between her, reviewers and the technical editor. This relieved the Principal Editor (the president) from a large amount of work and ensured a consistent standard from year to year.

Her presence at the meeting was only a small part of her contribution, however. Starting straight after the meeting with those manuscripts that had been submitted and continuing for the following 2 or 3 months, she would carefully go through each manuscript, correcting them to ensure that the English was comprehensible. In some cases this required corresponding with the authors to find out exactly what was meant in a particular sentence or paragraph. Her task was to keep her changes to a minimum, but on occasions she went beyond the call of duty and took on the challenge of entirely correcting almost incomprehensible manuscripts. In all of her work she was cheerful and constructive and her sense of humour came over in the many e-mails we exchanged during the editing process.

She was a key element in the team (the "dream team" she called it) that has edited the ISOTT volume for the last 15 years. All of us in ISOTT are grateful for her long service to the society. She will be sorely missed.
On behalf of ISOTT
David Harrison

ISOTT 2019 Awardees

Melvin H Knisely Award
Ting Li
Dietrich Lubbers Award
Kazuki Hotta
Britton Chance Award
Alexander Kalyanov
Bruley Awardees
Gary Angles
Tim Darlington
Min Feng
Thea Huesing
Bhabuk Koirala
Sho Kojima
Jonathan Nguyen
Labiblias Rahman
Mandy Rauschner
Aarti Sethuraman
Eileen Thiessen

ISOTT 2019 Sponsors

Kinesio
Vitech Bio
Clin EPR, LLC, Lyme, NH
Oxford Optronix
Scientica Instrumentation
Hamamatus
Fujifilm
Visualsonics

Contents

Part III Tumor Oxygenation and Modeling

Part I

Oxygen Metabolism and Health Monitoring

Chronic Ketosis Modulates HIF1α-Mediated Inflammatory Response in Rat Brain

1

Aarti Sethuraman, Prahlad Rao, Atul Pranay, Kui Xu, Joseph C. LaManna, and Michelle A. Puchowicz

Abstract

Hypoxia inducible factor alpha (HIF1α) is associated with neuroprotection conferred by diet-induced ketosis, but the underlying mechanism remains unclear. In this study, we use a ketogenic diet in rodents to induce a metabolic state of chronic ketosis, as measured by elevated blood ketone bodies. Chronic ketosis correlates with neuroprotection in both aged and following focal cerebral ischemia and reperfusion (via middle cerebral artery occlusion, MCAO) in mouse and rat models. Ketone bodies are known to be used efficiently by the brain, and metabolism of ketone bodies is associated with increased cytosolic succinate levels that inhibits prolyl hydroxylases allowing HIF1α to accumulate. Ketosis also regulates inflammatory pathways, and HIF1α is reported to be essential for gene expression of interleukin 10 (IL10). Therefore, we hypothesized that ketosis-stabilized HIF1α modulates the expression of inflammatory cytokines orchestrating neuroprotection. To test changes in cytokine levels in rodent brain, 8-week-rats were fed either the standard chow diet (SD) or the KG diet for 4 weeks before ischemia experiments (MCAO) were performed and the brain tissues were collected. Consistent with our hypothesis, immunoblotting analysis shows IL10 levels were significantly higher in KG diet rat brain compared to SD, whereas the TNFα and IL6 levels were significantly lower in the brains of KG diet-fed group.

Keywords

Ketone bodies · Hypoxia · Hypoxia inducible factors · Cytokines · Ischemic reperfusion

A. Sethuraman · P. Rao · A. Pranay
Department of Pediatrics, University of Tennessee Health Science Center, Memphis, TN, USA

K. Xu · J. C. LaManna
Department of Physiology & Biophysics, Case Western Reserve University, Cleveland, OH, USA

M. A. Puchowicz (✉)
Department of Pediatrics, University of Tennessee Health Science Center, Memphis, TN, USA

Department of Nutrition, Case Western Reserve University, Cleveland, OH, USA
e-mail: mpuchowi@uthsc.edu

1.1 Introduction

The mechanism through which diet-induced ketosis confers neuroprotection remains unclear despite its clinical applications for over seven decades [1]. Studies have implicated ketosis in modulating metabolic profiles and inflammatory pathways [1–3]. The ketogenic diet (KG) is a high-fat, very-low-carbohydrate diet which results in hepatic production of ketone bodies due

E. M. Nemoto et al. (eds.), *Oxygen Transport to Tissue XLII*, Advances in Experimental Medicine and Biology 1269, https://doi.org/10.1007/978-3-030-48238-1_1

to elevated beta-oxidation of fats by the liver. Ketosis results in elevated blood ketone bodies (beta-hydroxybutyrate and acetoacetate; BHB, AcAc) which are alternate energy substrates to glucose and are known to be well utilized by the brain, especially during glucose sparing conditions [3]. Ketones are beneficial substrates during metabolic derangements of glucose metabolism such as with ischemia/reperfusion injury-induced oxidative stress. The KG diet is a well-established non-pharmacological approach to treat drug-resistant epilepsy in children and has shown promise in treating other neurological conditions such as Alzheimer and stroke [4, 5].

We have consistently reported that ketosis induced by KG diet or by local intraventricular infusions of BHB correlates with neuroprotection following focal cerebral ischemia and reperfusion (via middle cerebral artery occlusion, MCAO) in rat (Fig. 1.1a, modified [2]) and mouse (data not shown), respectively [1, 2]. The metabolic adaptation to chronic ketosis and the mechanistic actions of ketosis in the brain (globally and cellular) are multifactorial but not well understood. Prolyl dehydrogenase (PHD)-mediated oxygen sensing and regulation of hypoxia inducible factors have been well studied, but normoxic regulation of this pathway warrants further study. This study focused on investigating the potential mechanisms associated with normoxic accumulation of hypoxia inducible factor-1 alpha (HIF1α) in diet-induced ketotic rats [1]. Specifically, we investigated the role of KG diet on inflammatory responses as associated with HIF1α stabilization in preconditioned ketotic rat brain. We targeted markers of pro- vs anti-inflammatory cytokines (TNFα and IL6 vs IL10) in cortical brain of ketotic rat to determine potential neuroprotective mechanisms mediated by HIF1α.

1.2 Methods

Animals: Experimental protocols were approved by the Institutional Animal Care and Use Committee (IACUC) at Case Western Reserve University (CWRU). Male: Two separate cohorts of Wistar male rats (8 weeks old) were fed either KG (high fat, carbohydrate restricted; $n = 4$) or standard lab chow (STD; $n = 4$) diets for 4 weeks before performing either focal cerebral ischemia (by MCAO) and infarct measurements or tissue collections (brain and blood), as previously described [1]. Rats were maintained on a 12:12 light-dark cycle with their diets and water available ad libitum. Diet Protocols: ketogenic (KG; 89.5 fat %, 10.4 protein %, 0.1 CHO %; Research

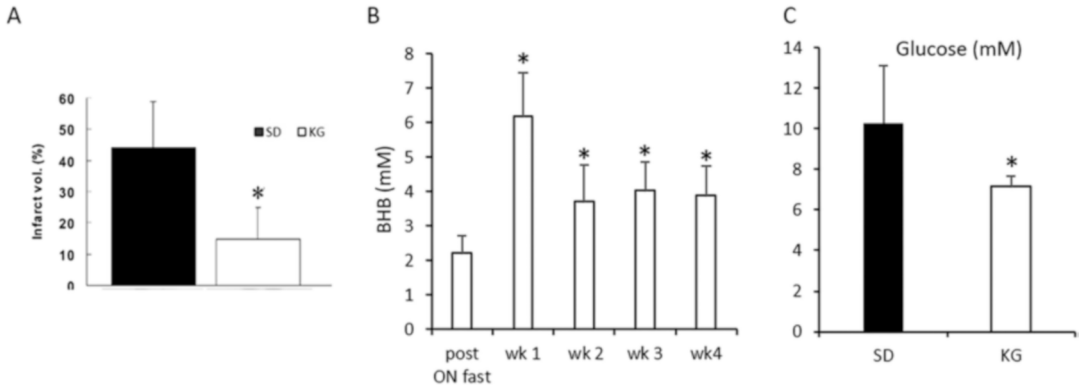

Fig. 1.1 (**a**) Infarct volumes in rat brains following MCAO were significantly lower in KG diet- vs SD diet-fed rats (modified from [2]). (**b**) Blood ketones (BHB) in rats fed with the ketogenic diet were measured with Precision Xtra® handheld keto-monitor. The blood ketone levels in KG-fed rats spiked the first week and stabilized in the following weeks. (**c**) Absolute glucose levels measured in blood plasma using GC-MS analysis show that glucose levels were elevated in the SD as compared to the KG diet-fed rats. The values presented are the mean ± S.E.M. ($n = 4$). * Denotes statistical significance ($p < 0.05$)

Diets, New Brunswick, NJ diet) and standard (STD; 27.5 fat %, 20.0 protein %, 52.6, provided by the CWRU animal facility). Weekly BHB concentrations were analyzed using a keto-meter (Precision Xtra, Abbott, Alameda California) from a small blood sample taken from the tail. *Metabolic Panels (Gas Chromatography Mass Spectrometry [GC-MS]-Based Analysis)*: Absolute glucose concentration (mM) was measured from blood plasma collected. The metabolite derivatives were assayed on an Agilent 5973N-MSD equipped with an Agilent 6890 GC system coupled to a DB-17MS capillary column (30 m × 0.25 mm × 0.25 μm) and operated in electron impact ionization mode [3]. *Western Blot Analysis*: Nuclear protein extracts prepared from cortical brain were immunoblotted using anti-HIF1α and anti-HIF2α antibodies and normalized to TBP, while the cytosolic protein extract was immunoblotted with anti-IL10, anti-IL6, and anti-TNFα and normalized to GAPDH, as previously described [6, 7]. Proteins were detected by chemiluminescence, and densitometric quantification was performed using ImageJ software. *Statistical Analysis*: All values were presented as mean ± SEM. Statistical analyses were performed using GraphPad Prism 7®. The comparison between any two groups was analyzed with a t-test for paired sample, two-tailed. Significance was considered at the level of $p < 0.05$.

1.3 Results

Blood Metabolites in KG and SD Diet-Fed Rats: Blood ketone levels in KG-fed rats spiked in the first week of diet to 6.2 mM and stabilized throughout the remaining weeks to an average of 3.9 mM (Fig. 1.1B). Absolute concentrations of plasma glucose were determined using GC-MS (Fig. 1.1C). Plasma glucose concentrations trended lower (but not statistically significant) in KG compared to SD diet group. *Diet-Induced Ketosis on HIF1α-Mediated Inflammatory Response*: Immunoblotting results (Fig. 1.2) show significantly higher protein levels of HIF1α in cortical brain of KG rats compared to SD group, while HIF2α levels remained unchanged between groups. Consistent with our hypothesis, IL10 levels were significantly higher in KG rat cortical brain compared to SD, while the TNFα and IL6 levels were significantly lower in KG group (Fig. 1.2B).

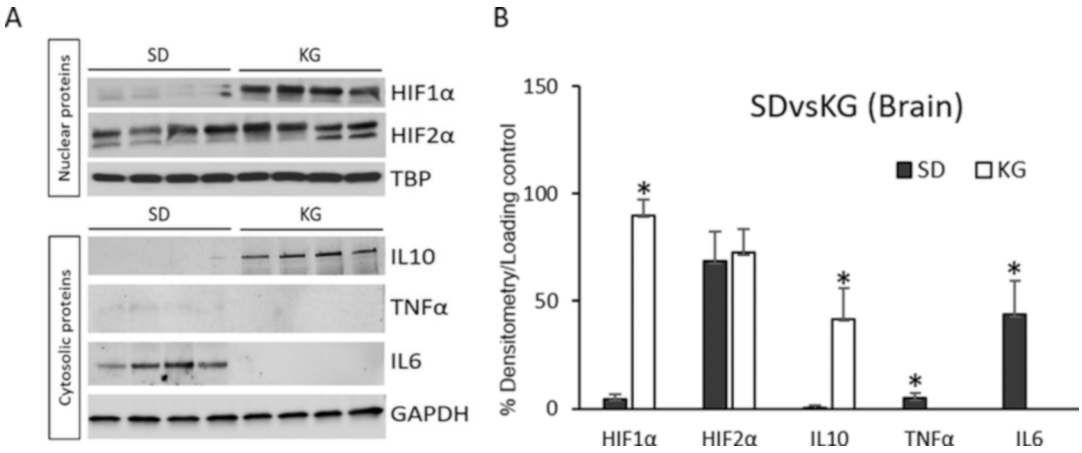

Fig. 1.2 (**a**) Western blot analysis of HIF1α, HIF2α, and cytokines IL10, TNFα, and IL6. HIF1α and HIF2α protein levels were normalized to TATA-box binding protein (TBP) loading control, while IL10, TNFα, and IL6 were normalized to GAPDH. (**b**) HIF2α protein levels remain unchanged, but HIF1α was significantly higher in KG rat brain. Expression of anti-inflammatory cytokine IL10 was significantly higher in KG brain, while no expression of pro-inflammatory cytokines IL6 and TNFα was observed. The values presented are the mean ± S.E.M. ($n = 4$). * Denotes statistical significance ($p < 0.05$)

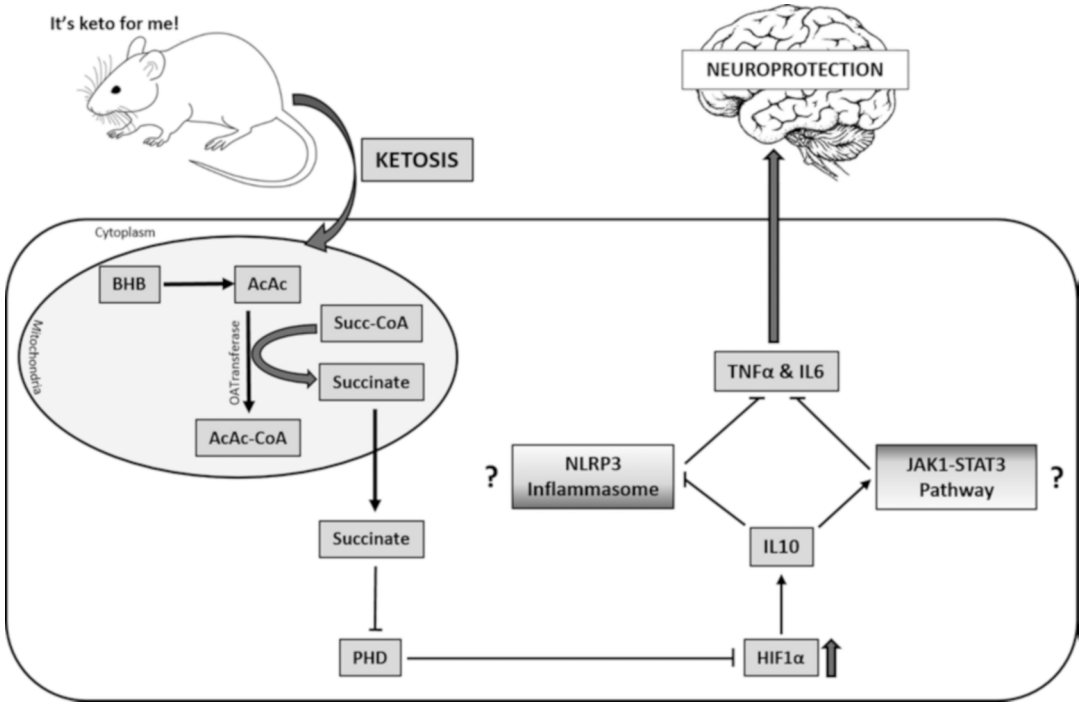

Fig. 1.3 Schematic model of our conclusion and future direction. Utilization of ketone bodies generated by metabolism of ketogenic diet as energy source causes accumulation of succinate on a cellular level in rat brains, which in turn inhibits prolyl hydroxylases resulting in accumulation of HIF1α. IL10, in turn, causes a downregulation of pro-inflammatory cytokines TNFα and IL6, leading to a neuroprotective phenotype. Further studies are needed to delineate the pathways involved in this downregulation (abbreviations used: AcAc, acetoacetate; BHB, β-hydroxybutyrate; CoA, coenzyme A; PHD, prolyl dehydrogenase; and Succ-CoA, succinyl-CoA)

1.4 Discussion

In this study, we show that normoxic stabilization of HIF1α in cortical ketotic rat brain is associated with modification of inflammatory cytokines which could confer neuroprotection following ischemic injury.

Diet-induced stabilization of HIF1α in rodent brain under normoxic ketotic conditions has been previously shown by Puchowicz et al. [1–3]. HIF1α can transcriptionally regulate IL10 levels by direct binding to hypoxia-responsive elements (HREs) on the IL10 promoter [8]. Further, overexpression of IL10 in mice has been associated with a resistance to ischemic injury (MCAO) [9]. Our study brings together ketosis-mediated stabilization of HIF1α and a potential neuroprotective phenotype in rats via IL10-mediated regulation of inflammatory cytokines. The inverse relationship we observe with HIF1α and IL6 levels has also been observed in a study by Schaefer et al. They reported HIF1α protein levels were higher under sustained hypoxia with a significant reduction in both mRNA and protein levels of IL6 [10].

IL10-meditated inflammatory pathways have been extensively studied for its implications in the design of targeted approaches aiming at controlling deleterious inflammation in the brain [11]. Our study connects to IL10-mediated immune regulation through downregulation of pro-inflammatory cytokines. One potential mechanism for this downregulation is via attenuation of the NLRP3 inflammasome as reported by Kanneganti et al. [12], thereby suspending activation of downstream pro-inflammatory cytokines like IL6 and TNFα. Secondly, IL10 receptor activation has been shown to specifically activate the JAK1-STAT3-mediated downregulation of pro-inflammatory cytokines [13]. Further, IL10-JAK1-STAT3 pathway has been described

as the negative regulator of inflammation that controls both the degree and duration of inflammation [14].

Figure 1.3 is a scheme of our model system; it depicts the mechanism for HIF1α stabilization by KG diet is through cellular metabolic redox signaling within the mitochondria. Specifically, succinate is an intermediate of ketone body catabolism which is generated at the level of the citric acid cycle following activation of AcAc to AcAc-CoA as coupled to the conversion of succinyl-CoA to succinate via CoA-transferase (OAT). To maintain metabolic redox, succinate is transported out of the mitochondria into cytosol where it acts to inhibit prolyl hydroxylases (PHD), thus resulting in HIF1α accumulation. Lastly, the molecular pathway involved in HIF1α-mediated downregulation of pro-inflammatory cytokines (IL6 and TNFα) is via IL10-mediated attenuation of the NLRP3 inflammasome or via IL10/JAK1/STAT3-mediated transcriptional attenuation. Thus, neuroprotection by ketosis involves modulation of the inflammatory response in the rat brain.

Acknowledgments This study was supported by NIH grant R01 NS 38632; Mouse Metabolic Phenotyping Consortium (*P&F 20497-21, MMPC*).

References

1. Puchowicz MA, Zechel JL, Valerio J et al (2008) Neuroprotection in diet-induced ketotic rat brain after focal ischemia. J Cereb Blood Flow Metab 28(12):1907–1916
2. Xu K, Ye L, Sharma K et al (2017) Diet-induced ketosis protects against focal cerebral ischemia in mouse. Adv Exp Med Biol 977:205–213
3. Zhang Y, Xu K, Kerwin T et al (2018) Impact of aging on metabolic changes in the ketotic rat brain: glucose, oxidative and 4-HNE metabolism. Adv Exp Med Biol 1072:21–25
4. Gasior M, Rogawski MA, Hartman AL (2006) Neuroprotective and disease-modifying effects of the ketogenic diet. Behav Pharmacol 17(5–6):431–439
5. Gibson CL, Murphy AN, Murphy SP (2012) Stroke outcome in the ketogenic state – a systematic review of the animal data. J Neurochem 123(Suppl 2):52–57
6. Sethuraman A, Brown M, Seagroves TN et al (2016) SMARCE1 regulates metastatic potential of breast cancer cells through the HIF1A/PTK2 pathway. Breast Cancer Res 18(1):81
7. Sethuraman A, Brown M, Krutilina R et al (2018) BHLHE40 confers a pro-survival and pro-metastatic phenotype to breast cancer cells by modulating HBEGF secretion. Breast Cancer Res 20(1):117
8. Cai Z, Luo W, Zhan H et al (2013) Hypoxia-inducible factor 1 is required for remote ischemic preconditioning of the heart. Proc Natl Acad Sci U S A 110(43):17462–17467
9. Garcia JM, Stillings SA, Leclerc JL et al (2017) Role of Interleukin-10 in acute brain injuries. Front Neurol 8:244
10. Schaefer E, Wu W, Mark C et al (2017) Intermittent hypoxia is a proinflammatory stimulus resulting in IL-6 expression and M1 macrophage polarization. Hepatol Commun 1(4):326–337
11. Lobo-Silva D, Carriche GM, Castro AG et al (2016) Balancing the immune response in the brain: IL-10 and its regulation. J Neuroinflammation 13(1):297
12. Gurung P, Li B, Subbarao Malireddi RK et al (2015) Chronic TLR stimulation controls NLRP3 inflammasome activation through IL-10 mediated regulation of NLRP3 expression and caspase-8 activation. Sci Rep 5:14488
13. Verma R, Balakrishnan L, Sharma K et al (2016) A network map of Interleukin-10 signaling pathway. J Cell Commun Signal 10(1):61–67
14. Hutchins AP, Diez D, Miranda-Saavedra D (2013) The IL-10/STAT3-mediated anti-inflammatory response: recent developments and future challenges. Brief Funct Genomics 12(6):489–498

2 Event-Related NIRS and EEG Analysis for Mental Stress Monitoring

Labiblais Rahman, Katsunori Oyama, Atsuhiro Tsubaki, and Kaoru Sakatani

Abstract

Mental disorders caused by chronic stress are difficult to identify, and colleagues in the work environment may suddenly report symptoms. Social barriers exist including the financial cost of medical services and the lack of a perceived need for treatment even if potential patients have a desire to receive mental healthcare. Self-report inventories such as the Beck Depression Inventory (BDI-II) and State-Trait Anxiety Inventory (STAI) can assess the emotional valence for mental health assessment, but medical expertise may be required for interpretation of the results. Contingency plans for clinical supervision and referral sources are necessary for sufficient mental healthcare using self-report inventories. On the other hand, the laterality index at rest (LIR) has been proposed for evaluation of the mental stress level from near-infrared spectroscopy (NIRS) data in the prefrontal cortex in the resting state. However, the potential for long-term monitoring has not been investigated with sufficient evaluation results. In this study, feature values were extracted from both NIRS and EEG signals each week for 10 weeks in four young participants with an average BDI-II score of 17.7, i.e., indicative of mild depression. Temporal changes in LIR and heart rate (HR) were compared with STAI-Y1 and BDI-II scores. We found cross-correlations between the time series of LIR and STAI-Y1 within one-week delay. In addition, the time series of LIR was also correlated with BDI-II with one-week delay. Importantly, by annotating the larger changes in LIR and HR on daily life events, the changes in LIR and HR were different depending on the type of life event that affected these moods.

Keywords

NIRS · Mood disorder · Health monitoring · Laterality index at rest

L. Rahman
Graduate School of Computer Science, Nihon University, Tokyo, Japan

K. Oyama (✉)
Department of Computer Science, College of Engineering, Nihon University, Tokyo, Japan
e-mail: oyama.katsunori@nihon-u.ac.jp

A. Tsubaki
Institute for Human Movement and Medical Sciences, Niigata University of Health and Welfare, Niigata, Japan

K. Sakatani
Department of Human and Engineered Environmental Studies, The University of Tokyo, Tokyo, Japan

E. M. Nemoto et al. (eds.), *Oxygen Transport to Tissue XLII*, Advances in Experimental Medicine and Biology 1269, https://doi.org/10.1007/978-3-030-48238-1_2

2.1 Introduction

For health monitoring, near-infrared spectroscopy (NIRS) can be used to monitor the hemodynamic response to mental stress for early detection of unusual changes related to various types of illnesses. Recent studies have identified the prefrontal cortex (PFC) as a key region that is involved in the experience and regulation of emotional responses [1]. State anxiety (STAI-Y1), a subscale of the State-Trait Anxiety Inventory, is one of the useful inventories for tracking changes of the emotional valence for health monitoring. STAI-Y1 ranges between 20 and 80 with 20 questions. STAI-Y1 can be estimated from the laterality index at rest (LIR) of oxyhemoglobin concentration changes using a machine learning algorithm [2]. LIR was originally developed for objective assessment of mental stress levels by measuring changes in the hemoglobin concentration in the bilateral PFCs at rest [3, 4]. LIR can also be applied from the laterality of electroencephalogram (EEG) alpha-band powers in the bilateral PFCs at rest, which is known as frontal alpha asymmetry (FAA). A recent finding from an EEG study is that FAA is conditionally correlated with the Beck Depression Inventory (BDI-II) score [5]. The BDI-II score ranges from 0 to 63 with 21 questions, and each question is assigned with four answers marked as 0 through 3.

However, LIR has rarely been applied for assessment of daily changes in emotional valence, due to the burden of using NIRS equipment or EEG sensors for a long period of time. The values of LIR extracted from the NIRS signals may be physiologically related to FAA and heart rate (HR), although these parameters have not been compared with sufficient conditions. On the other hand, self-report inventories such as STAI-Y1 and BDI-II are difficult to use with continuous monitoring of life events such as stress factors including major disasters and changes in human relations. These self-report inventories are not designed for checking such changes.

The health monitoring approach in this study aims to explore the potential of the periodic use of NIRS for long-term mental stress monitoring. The main contribution of this study is the application of LIR to find unusual changes in emotional valence, including depression risk and anxiety symptoms.

2.2 Methods

In this study, LIR needed to be obtained at an arbitrary time during the resting state. Therefore, calculation of LIR was automated by taking into consideration the temporal change for k seconds in the resting state (Fig. 2.1). Concentration changes in oxyhemoglobin during measurement of the right and left PFCs are assigned the variables $h_{\mathrm{r}}(t)$ and $h_{\mathrm{l}}(t)$, respectively. The values $h_{\mathrm{r\_min}}$ and $h_{\mathrm{l\_min}}$ are the minimum values during the measurement for k seconds. LIR for k seconds as the difference between the changes in hemodynamic responses of $h_{\mathrm{r}}(t)$ and $h_{\mathrm{l}}(t)$ is then averaged:

$$\mathrm{LIR} = \frac{1}{k}\sum_{t=0}^{k}\frac{\left(h_{\mathrm{r}}(t)-h_{\mathrm{r\_min}}\right)-\left(h_{\mathrm{l}}(t)-h_{\mathrm{l\_min}}\right)}{\left(h_{\mathrm{r}}(t)-h_{\mathrm{r\_min}}\right)+\left(h_{\mathrm{l}}(t)-h_{\mathrm{l\_min}}\right)}$$

FAA is obtained from the difference in EEG alpha power between the right and left frontal regions. In this study, the FAA is averaged during the resting state. Spectral powers between 8 and 12 Hz at the right and left PFCs are assigned to $s_{\mathrm{r}}(t)$ and $s_{\mathrm{l}}(t)$, respectively. In this experiment, $s_{\mathrm{r}}(t)$ denotes averaged alpha power at a discrete time t in the electrode positions of FP2 and F4 over the right hemisphere, whereas $s_{\mathrm{l}}(t)$ is the average alpha power in the electrode positions of FP1 and F3 over the left hemisphere. Each epoch to obtain alpha power is 60 seconds long, and FAA for k seconds is then averaged:

$$\mathrm{FAA} = \frac{1}{k}\sum_{t=0}^{k}\frac{s_{\mathrm{r}}(t)-s_{\mathrm{l}}(t)}{s_{\mathrm{r}}(t)+s_{\mathrm{l}}(t)}$$

In this experiment, we studied four young participants (two males and two females; ages between 23 and 26 with average BDI-II score of 17.7) as shown in Table 2.1, i.e., indicative of mild depression, who participated in this experiment at noon on every Monday, Wednesday, and Friday for

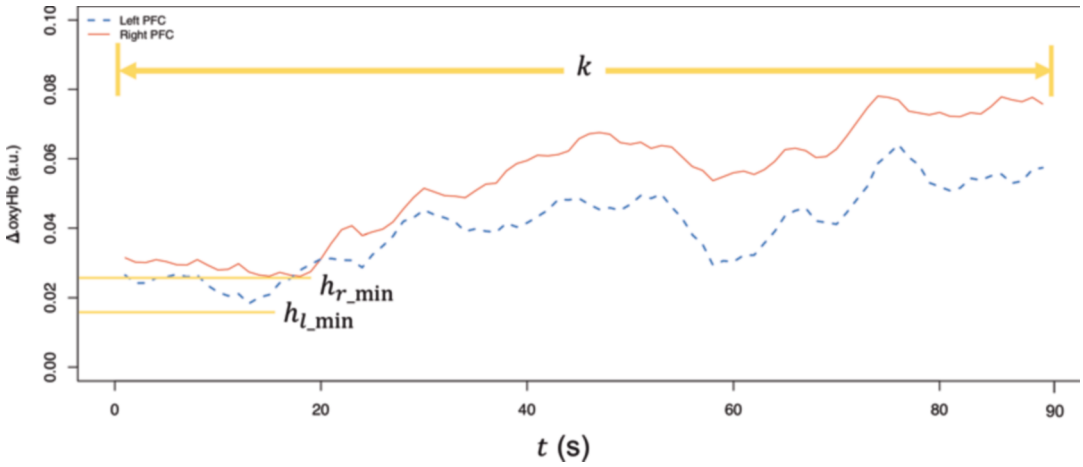

Fig. 2.1 Acquisition of parameters for extraction of the value of LIR

over 10 weeks. We evaluated the emotional valence for each participant using the STAI-Y1 and BDI-II tests. Recordable life events during the experiment, such as "trouble at a holiday party," were collected in their daily journals along with the results of BDI-II and STAI-Y1 tests. Before each measurement, the participants reported their body conditions, e.g., hours of sleep and meal time. We measured the changes in oxyhemoglobin concentration in the bilateral PFCs in the resting condition using a Pocket NIRS (Hamamatsu Photonics K.K., Japan). FAA was measured with Open BCI EEG sensors. Each measurement was conducted as follows: (1) EEG signals were recorded in the resting state with the eyes closed for 90 seconds, (2) then NIRS signals were recorded in the same manner, and (3) the participants filled in the forms of STAI-Y1 and BDI-II and wrote comments in their daily journal. HR data were measured throughout the experiment with smart watches (Fig. 2.2).

2.3 Results

Cross-correlation function (CCF) was employed for correlation analysis on the time series data from the experimental results. In this analysis, cross-correlation was calculated from the weekly changes of LIR, FAA, HR, STAI-Y1, and BDI-II. Note that these weekly changes were standardized by standard deviations to compare their temporal changes. From the experimental results, the changes in LIR and FAA were conditionally correlated with STAI-Y1 and BDI-II scores; however, depending on how the participants answered the self-report inventories, time lags of 1 week can be found as the correlation coefficients in bold shown in Tables 2.2 and 2.3. The changes in HR mostly followed after the changes in LIR and FAA. For example, the change in BDI-II score of Participant 1 is delayed nearly a week from the change in LIR, as shown in Fig. 2.3. Participant 1 had a BDI-II score of 20, which is on the border between mild and moderate depression according to the cutoff value of 20. LIR and FAA fluctuated during the life events such as "Trouble at a holiday party," as shown in Figs. 2.3 and 2.4. On the other hand, similar change patterns can be found after this period.

Participant 1 had a BDI-II score of 20, which is on the border between mild and moderate depression according to the cutoff value of 20. The values of LIR, FAA, and HR fluctuated during life events such as "Trouble at a holiday party." On the other hand, moderate changes were found during the life event "Winter break." Note that the values in Figs. 2.3 and 2.4 are standardized by standard deviations.

Table 2.1 Statistical summary: feature values (Ave. ± SD) obtained

	Age	Sex	LIR	FAA	HR	BDI	STAI Y1	# of sample data
Participant 1	23	F	0.099 ± 0.191	−0.046 ± 0.01	76 ± 16.5	20 ± 8	43.8 ± 5.1	24
Participant 2	26	F	−0.021 ± 0.221	−0.049 ± 0.041	99.4 ± 5.6	13.2 ± 4.5	49 ± 6.4	23
Participant 3	23	M	0.091 ± 0.208	−0.065 ± 0.026	85 ± 5.2	7.1 ± 6.1	43.3 ± 0.8	23
Participant 4	23	M	0.066 ± 0.203	−0.041 ± 0.028	93.9 ± 6.9	30.3 ± 2.2	40.4 ± 2.4	21

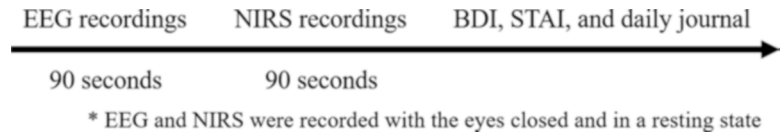

Fig. 2.2 Experimental protocol

Table 2.2 Cross-correlations with STAI scores with time lags of 1 week

	LIR			FAA			HR		
	lag −1	lag 0	lag 1	lag −1	lag 0	lag 1	lag −1	lag 0	lag 1
Participant 1	0.29	0.22	**0.40**	−0.25	**0.49**	0.04	−0.18	**0.62**	−0.15
Participant 2	**0.57**	−0.52	0.40	**0.39**	−0.83	0.21	−0.24	**0.37**	−0.16
Participant 3	**0.33**	−0.04	−0.13	−0.34	**0.41**	−0.54	−0.63	−0.03	**0.34**
Participant 4	−0.06	0.18	−0.67	−0.32	**0.53**	−0.17	−0.31	**0.55**	−0.05

Table 2.3 Cross-correlations with BDI-II scores with time lags of 1 week

	LIR			FAA			HR		
	lag −1	lag 0	lag 1	lag −1	lag 0	lag 1	lag −1	lag 0	lag 1
Participant 1	**0.54**	−0.06	0.13	−0.13	**0.19**	−0.09	−0.24	**0.66**	−0.08
Participant 2	−0.49	**0.91**	−0.67	−0.18	**0.40**	−0.33	0.03	−0.28	**0.71**
Participant 3	**0.66**	0.19	−0.29	−0.32	−0.14	−0.03	−0.21	−0.05	0.18
Participant 4	−0.13	0.15	0.15	−0.32	0.01	−0.06	−0.15	−0.50	0.16

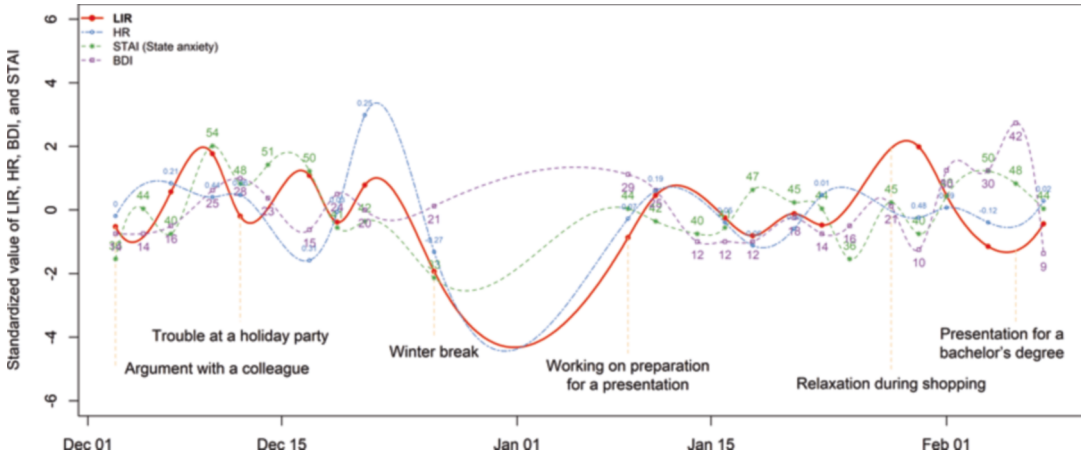

Fig. 2.3 Participant 1: Temporal changes of LIR to be compared with the feature values of HR, STAI-Y1, and BDI-II

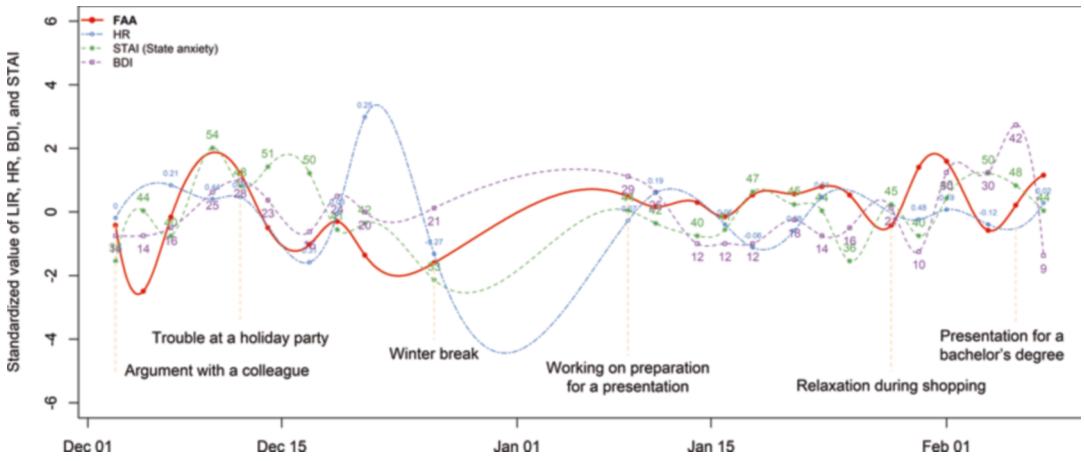

Fig. 2.4 Participant 1: Temporal changes of FAA to be compared with the feature values of HR, STAI-Y1, and BDI-II

2.4 Discussion

The experimental results suggest that both LIR and FAA can be feature values for assessment of daily changes in emotional valence; however, these results require further analysis with sample data obtained over longer periods so that a regression model can be developed to detect unusual change. This study was performed with the assumption that users can easily put on the wearable sensors in the home setting. In this experiment, NIRS signals were recorded just 90 seconds to extract the values of LIR, and we found that 90 seconds of measurement is sufficient in the home setting. Further improvement in the sensor equipment and measurement methods may have a large impact on the success of long-term monitoring.

In this paper, we discussed the applicability of LIR for the assessment of emotional valence. From the experimental result obtained with periodic NIRS recordings, LIR was compared with STAI-Y1 and BDI-II scores. We found cross-correlations between LIR and STAI-Y1 scores and between LIR and BDI scores. These observations provide rich information for the mental stress monitoring.

Future investigations will involve the development of a user-interface system that provides estimated STAI-Y1 and BDI scores for efficient health monitoring. The experimental results also suggest the potential for detection of unusual changes in emotional valence. Optimization of the method may eventually allow early detection of depression risk and anxiety symptoms.

References

1. Balconi M, Grippa E, Vanutelli ME (2015) What hemodynamic (fNIRS), electrophysiological (EEG) and autonomic integrated measures can tell us about emotional processing. Brain Cogn 95:67–76
2. Fukuda Y et al (2014) A Bayesian algorithm for anxiety index prediction based on cerebral blood oxygenation in the prefrontal cortex measured by near infrared spectroscopy. IEEE J Transl Eng Health Med 2:1–10
3. Davidson RJ, Jackson DC, Kalin NH (2000) Emotion, plasticity, cortex, and regulation: perspectives from affective neuroscience. Psychol Bull 126(6):890–909
4. Ishikawa W, Sato M, Fukuda Y, Matsumoto T, Takemura N, Sakatani K (2014) Correlation between asymmetry of spontaneous oscillation of hemodynamic changes in the prefrontal cortex and anxiety levels: a near-infrared spectroscopy study. J Biomed Opt 19(2):027005
5. Allen JJ, Reznik SJ (2015) Frontal EEG asymmetry as a promising marker of depression vulnerability: summary and methodological considerations. Curr Opin Psychol 4:93–97

3 Simulation Study of Breast Cancer Lipid Changes Affecting Membrane Oxygen Permeability: Effects of Chain Length and Cholesterol

Qi Wang, Rachel J. Dotson, Gary Angles, and Sally C. Pias

Abstract

Tumor radiotherapy relies on intracellular oxygen (O_2) to generate reactive species that trigger cell death, yet hypoxia is common in cancers of the breast. De novo lipid synthesis in tumors supports cell proliferation but also may lead to unusually high levels of the 16:1 palmitoleoyl (Y) phospholipid tail, which is two carbons shorter than the 18:1 oleoyl (O) tail abundant in normal breast tissue. Here, we use atomic resolution molecular dynamics simulations to test two hypotheses: (1) the shorter, 16:1 Y, tail of the de novo lipid biosynthesis product 1-palmitoyl,2-palmitoleoyl-phosphatidylcholine (PYPC) promotes lower membrane permeability relative to the more common lipid 1-palmitoyl,2-oleoylphosphatidylcholine (POPC), by reducing oxygen solubility in the interleaflet region, and (2) cholesterol further lessens the permeability of PYPC by reducing overall O_2 solubility and promoting PYPC tail order adjacent to the rigid cholesterol ring system. The simulations conducted here indicate that PYPC has a permeability of 14 ± 1 cm/s at 37 °C, comparable to 15.4 ± 0.4 cm/s for POPC. Inclusion of cholesterol in a 1:1 ratio with phospholipid intensifies the effect of chain length, giving permeabilities of 10.2 ± 0.2 cm/s for PYPC/cholesterol and 11.0 ± 0.6 cm/s for POPC/cholesterol. These findings indicate that PYPC may not substantially influence membrane-level oxygen flux and is unlikely to hinder breast tissue oxygenation.

Keywords

Molecular dynamics simulation · Hypoxia · Cholesterol · De novo lipid · Fatty acid biosynthesis

3.1 Introduction

Hypoxia is a common attribute of the tumor microenvironment [1]. Yet, tumor radiotherapy relies on intracellular O_2 to generate reactive oxygen radicals that damage DNA and lead to cell death [2, 3]. Thus, factors affecting the intracellular oxygen content of tumor cells are of interest for predicting and enhancing radiotherapy outcomes. This study addresses the possible influence of de novo fatty acids and cholesterol in breast tumors on intracellular oxygenation. Specifically, atomistic molecular dynamics simu-

Q. Wang · R. J. Dotson · G. Angles · S. C. Pias (✉)
Department of Chemistry, New Mexico Institute of Mining and Technology (New Mexico Tech), Socorro, NM, USA
e-mail: sally.pias@nmt.edu

E. M. Nemoto et al. (eds.), *Oxygen Transport to Tissue XLII*, Advances in Experimental Medicine and Biology 1269, https://doi.org/10.1007/978-3-030-48238-1_3

lations are used to examine membrane-level effects of lipid chain length and cholesterol on oxygen permeability, as well as solubility and diffusion within model membranes. Atomistic simulations enable precise control over lipid composition, along with subnanometer and picosecond timescale resolution. Prior simulation and experimental studies indicate that lipid compositional variations alter membrane oxygen permeability, as well as the pathway of oxygen diffusion [4–8].

The common membrane phospholipid 1-palmitoyl-2-oleoyl-phosphatidylcholine (POPC), or PC(16:0,18:1), has hydrocarbon tails that are well matched in chain length. Though its two tails differ in the number of carbons, the 16:0 saturated tail extends to roughly the same length as the 18:1 monounsaturated tail. Here, we use a conventional notation that specifies the number of carbons in the tail, *n*, followed by the number of *cis* double bonds, *x*, giving *n*:*x*.

De novo fatty acid biosynthesis is typically upregulated in cancers, and the new fatty acids are used to build membranes for cell proliferation [9]. Products of de novo lipid biosynthesis are unusually abundant in breast cancer cells [10]. In particular, the cell membranes of poor-prognosis breast tumors appear to contain high levels of the 16:1 palmitoleoyl (Y) fatty acyl tail, which can form 1-palmitoyl-2-palmitoleoyl-phosphatidylcholine (PYPC) [9]. The POPC and PYPC lipids are identical in structure, except that the unsaturated tail of PYPC is two carbons shorter than that of POPC. We anticipated that the shorter tail would introduce chain-length mismatch and, therefore, would promote tail interdigitation at the leaflet–leaflet interface. As such, the first hypothesis tested in this study is that the shorter, 16:1 Y, tail of PYPC promotes lower membrane permeability relative to POPC, by reducing oxygen solubility in the interleaflet region.

The study also examines the effects of cholesterol (chol) in combination with PYPC, as cholesterol modifies the free energy landscape of oxygen translocation in POPC and promotes oxygen solubility in the interleaflet region [6]. Cholesterol accounts for 20–40% of the membrane lipid molecules in most cell types and occurs at higher levels in the eye lens [8, 11] and in red blood cells (RBCs). The RBC membrane cholesterol-to-phospholipid ratio is typically 1:1 (50 mol% cholesterol) [12]. We previously found that POPC bilayer O_2 permeability decreases when cholesterol is enriched [6], and this finding is consistent with experiment [8]. The O_2 lipid–water partition coefficient (or relative solubility) is reduced roughly in proportion to the permeability decrease in POPC/chol [13], as predicted by Overton's rule [14]. Cholesterol reduces the solubility of oxygen within the bilayer, as a whole, but increases the solubility locally in the interleaflet region [6]. The second hypothesis tested in this study is that cholesterol further lessens the permeability of PYPC by reducing overall O_2 solubility and promoting PYPC tail order adjacent to the rigid cholesterol ring system.

The oxygen permeability and related properties are studied for PYPC alone and with 50% cholesterol. Comparison is made to POPC alone and with 50% cholesterol. The 50% cholesterol level (1:1 mixing ratio) was chosen because permeability changes were previously observed at and above this level [6, 8].

3.2 Methods

All-atom molecular dynamics (MD) simulations were carried out with graphics processing unit (GPU)-enabled AMBER code, version 14 [15, 16]. The Lipid14 force field, cholesterol extension, and TIP3P water model were applied [17–19]. The pressure was fixed at 1 bar using the Monte Carlo barostat with anisotropic scaling, and the temperature was maintained at 310 K using the Langevin thermostat with a collision frequency of 1 ps^{-1}. Bonds to hydrogen were constrained with SHAKE [6]. The simulation timestep was 2 fs, with coordinates written every 1 ps. Periodic boundary conditions were applied, and particle-mesh Ewald was used to calculate nonbonding interactions, with a cutoff distance of 10 Å.

Four simulation systems were constructed: PYPC, POPC, PYPC/chol (1:1 mixing ratio, or 50 mol% cholesterol), and POPC/chol.